FULafia Journal of Science & Technology
ISSN (print) 2449-0954 \ ISSN (online) 2636-4972
https://lafiascijournals.org.ng/index.php/fjst
Sponsored By TETFUND TERTIARY EDUCATION TRUST FUND
Manuscript => Received: Jan., 2026; **Accepted:** May, 2026; **Published:** May, 2026 https://doi.org/10.62050/fjst2026.v10n2.785

DYNAMICS OF FLOW AND HEAT TRANSFER MECHANISM OF HYDROMAGNETIC MAXWELL FLUID OVER A SPINNING DISK WITH MARANGONI EFFECTS

Ephesus O. Fatunmbi* and Olusegun A. Olaiju
Department of Mathematics and Statistics, Federal Polytechnic Ilaro, Nigeria
*Corresponding email: ephesus.fatunmbi@federalpolyilaro.edu.ng

ABSTRACT
Investigating the flow of non-Newtonian fluids influenced by a magnetic field is important to improve current thermal systems through different technologies. Typical of these applications can be found in polymer processing devices, rotating equipment, microfluidic devices, and cooling mechanisms. The goal of this paper is to investigate the dynamics of flows and heat-mass transfer mechanism of hydromagnetic Maxwell fluids over a rotating disk featuring Marangoni convection, thermal radiation, and bioconvection effects. The initially developed model equations are restructured into ordinary differential equations and solved numerically by shooting and Runge-Kutta Felhberg method. The findings which are reported through various graphs indicate that there is a decline in the velocity field with increasing fluid material parameter and porous medium resistance, whereas the temperature field intensifies in the with magnification of thermophoresis, thermal radiation, and Brownian motion terms. Furthermore, the viscoelastic nature of the Maxwell nanofluid enhances resistance to deformation, thereby reducing momentum transport and providing a mechanism for regulating fluid elasticity and improving heat transfer along the disk surface.

Keywords: Maxwell nanofluid, Thermal radiation, Marangoni effects, Spinning disk.

INTRODUCTION
The magnetohydrodynamic (MHD) flows of non-Newtonian fluids have received much research in fluid dynamics due to their many applications in industrial and engineering areas. Typical of such applications are in food processing, polymer extrusion, biomedical engineering, and so many others (Mustafa *et al*., 2027; Alrihieli, *et al*., 2025). One of the most important classes of non-Newtonian viscoelastic fluids is a Maxwell fluid. This model represents many types of polymeric liquids or plastics that have properties which behave in an elastic manner, including some biological fluids. When a non-Newtonian viscoelastic Maxwell fluid is exposed to external magnetic fields, the electrically conducting nature of the flowing fluid creates a Lorentz force acting on the fluid, changing the fluid velocity profile and consequently enhancing the flow structure. MHD fluid flow characteristics of Maxwell fluids are significant in many of the technological processes such as polymer extrusion, electronic cooling, metallurgy, petroleum recovery and MHD power generation. Thus, several authors have examined such phenomena using the Maxwell fluids. For instance, Megahed (2021) reported heat enhancement mechanism of the Maxwell fluid motion over a convectively heated elongating sheet. Abdelsalam *et al*. (2023) assessed rheological properties of the Maxwell fluid over a permeable expanding surface while Salawu *et al*. (2021) evaluated MHD transport of heat-mass transfer in the flow of the Maxwell fluid with Arrhenius activation energy, whereas Fatunmbi and Agbolade (2023) analyzed thermal convection in the magnetized non-Newtonian Maxwell fluid over a stretching surface. Meanwhile, when the Maxwell fluid is combined with nanofluid, an enhanced heat transfer is obtained.

The study of nanofluid transport over rotating or spinning surfaces has attracted considerable attention in thermal engineering due to its relevance in many emerging technological systems. Such flow configurations frequently arise in microelectromechanical systems, biomedical microfluidic platforms, chemical processing units, modern cooling technologies, and solar energy devices. The concept of *nanofluids* was originally introduced by Choi and Eastman (1995), who demonstrated that dispersing nanoscale solid particles into conventional base fluids can considerably improve their thermal performance. Numerous other investigations have validated the superior heat transfer potential of nanofluids with respect to conventional fluids (Mahian *et al*., 2019; Huminic & Huminic, 2020; Fatunmbi & Salawu, 2022). Some of the factors responsible for the superior thermal characteristics of nanofluids are due to the presence of mechanism like Brownian motion of the nanoparticles coupled with thermophoretic diffusion,

and the enhanced thermal conductivity of the nanofluids. To further understand the transport mechanisms of nanofluids, a general model for the convective flow of nanofluids was developed by Buongiorno (2006). An alternative model for the analysis of nanofluids was proposed by Tiwari and Das (2007). Since the publication of the initial study on nanofluid flow, numerous other researchers have tried to study the flow of nanofluids with different geometries and physical conditions, thereby establishing the significance of nanofluids in modern thermal and fluid systems (Fatunmbi *et al*., 2023; Yahaya *et al*., 2024; Acharya *et al*., 2022).

Research has indicated that thermal radiation plays a key role in heat transfer particularly in electrically conductive viscoelastic nanofluids, and also alters the boundary thickness when exposed to a magnetic field. In the studies conducted by Fatunmbi and Adeniyan (2020, 2018), they examined MHD micropolar and magneto-viscoelastic flows over stretching surfaces, and found that thermal radiation and viscous dissipation play a very important role in energy transport and in determining the boundary structure. Nasir *et al*. (2024) examined the concept of radiative fluid flow over a Riga Plate. The authors stated that thermal performance in many engineering systems can be achieved with proper management of radiative heat transfer. Guo *et al*. (2024) conducted research on thermal management strategy with effects of thermal radiation. It was reported that optimization of heat dissipation and improved thermal efficiency can be achieved by proper control of radiative energy system.

Moreover, the complexities of the boundary layer flow can also be enhanced through the incorporation of the Marangoni convection due to surface tension gradient induced by temperature or concentration differences. Alsallami *et al*. (2020) demonstrated the significant influence of the Marangoni force on the flow behavior and heat transfer characteristics over stretching surfaces. Liu *et al*. (2019) indicated the potential of the thermocapillary convection to produce high shear stress, leading to the interfacial flow over the rotating surface. The presence of the gyrotactic microorganisms in the bioconvective nanofluids causes the instabilities in the bioconvection, leading to the enhancement of the nanoparticle dispersion and the heat/mass transfer processes, as discussed in the studies of Wang *et al*. (2016), Gul *et al*. (2021), Fatunmbi *et al*. (2023), and Chebaane *et al*., 2025).

Despite the extensive studies on nanofluid flows, many vital gaps exist. Most studies consider a subset of the pertinent physics, characteristically ignoring the simultaneous relations among MHD effects, porous medium, thermal radiation, Brownian and thermophoretic diffusion, Marangoni thermocapillarity, and gyrotactic bioconvection, Additionally, spinning disk flows with coupling multi-physics remain limited, despite their widespread usage in industrial and solar thermal systems. Therefore, the need for an inclusive model integrating all these multifaceted effects into a single framework is evident. Motivated by the research applications and gaps, this study presents MHD radiative Maxwell nanofluid flow, and heat-mass transfer mechanism over a porous rotating disk with Marangoni convection, and gyrotactic microorganisms. This analysis provides insight into the multiphysics relations governing velocity, thermal, species, and density of microorganismin spinning nanofluid environments.

MATERIALS AND METHODS

Firstly, the assumptions for the development of the controlling equations are stated under this section. Following that is the formulation of the model equations using the conservative laws based on the assumptions stated. Subsequently, the introduction of the similarity transformation quantities for converting the governing equations from partial to ordinary derivatives, and finally, the description of the method of solution to the model equations.

Problem Formulation Assumptions

These assumptions are proposed for the development of the model equations:

The fluid motion is non-transient, and incompressible in nature. The working fluid is non-Newtonian Maxwell fluid and consists of tiny nanoparticles. The transport phenomenon is configured in a porous spinning disk subjected to Marangoni surface effects. A cylindricalcoordinate (r, φ, z) is employed for the model formulation. The plane of the disk is aligned with the $z - axis$ with an imposed magnetic field of strength B_0 fixed inclination angle ω to the normal of the disk as depicted in Fig. 1. The Bongiorno model of nanoparticles is used for the development of the nanoparticle's inclusion in the governing equations.

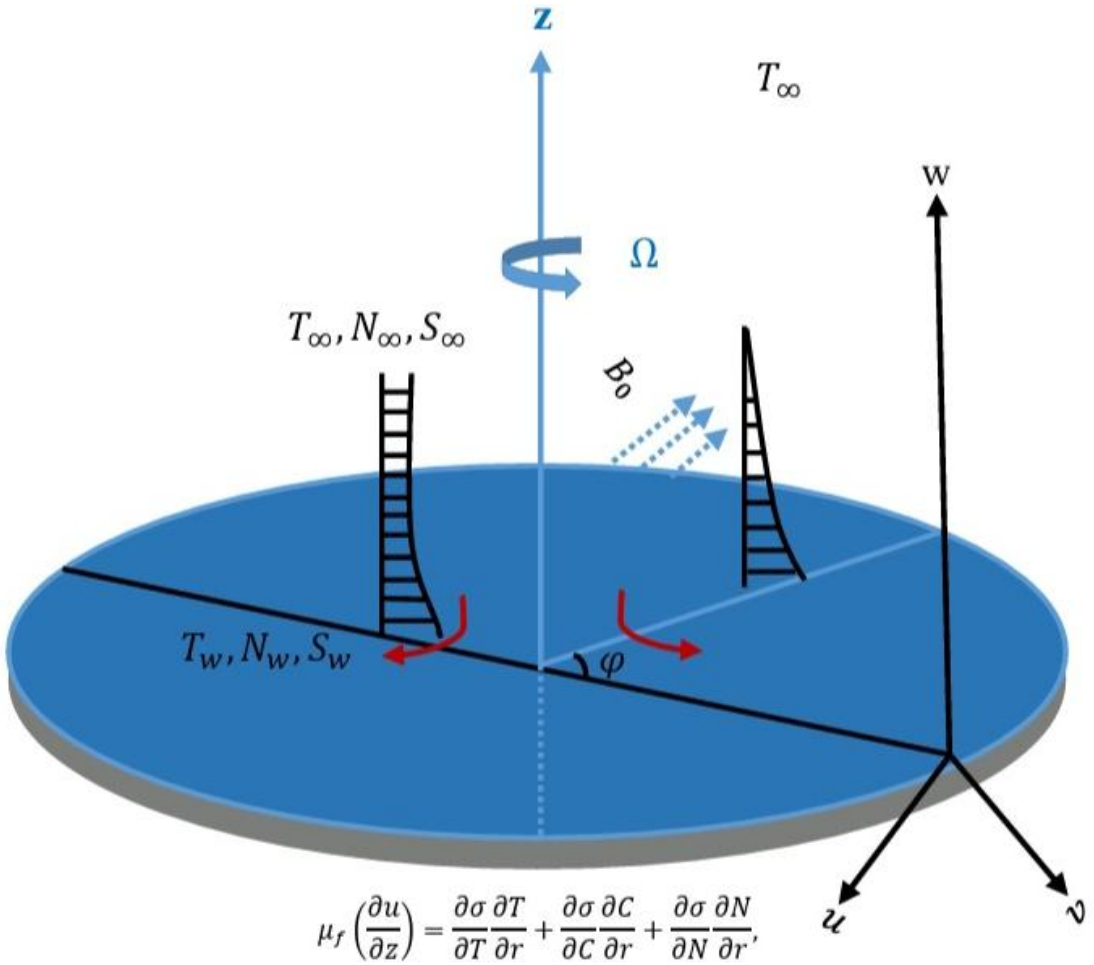

$$\mu_f\left(\frac{\partial u}{\partial z}\right)=\frac{\partial\sigma}{\partial T}\frac{\partial T}{\partial r}+\frac{\partial\sigma}{\partial C}\frac{\partial C}{\partial r}+\frac{\partial\sigma}{\partial N}\frac{\partial N}{\partial r},$$

$$v=nr, w=0, -k\frac{\partial T}{\partial z}=h_f\left(T_f-T\right), C=C_w, N=N_w$$

Figure 1: The nanofluid flow sketch along a rotating disk surface

The Governing Equations

By the use of conservation laws and the highlighted basic assumptions, the following equations are derived (Devi & Mabood, 2020):

$$\frac{\partial u}{\partial r}=-\left(\frac{\partial w}{\partial z}+\frac{u}{r}\right) \quad \#(1)$$

$$u\frac{\partial u}{\partial r}+w\frac{\partial u}{\partial z}-\frac{v^2}{r}=-\lambda_1 M_x+\nu_f\frac{\partial^2 u}{\partial z^2}-\left(\frac{\nu_f}{K^*}u+\frac{\sigma B_0^2}{\rho_f}u\right)\#(2)$$

$$u\frac{\partial v}{\partial r}+w\frac{\partial v}{\partial z}+\frac{uv}{r}=-\lambda_1 M_y+\nu_f\frac{\partial^2 v}{\partial z^2}-\left(\frac{\nu_f}{K^*}v+\frac{\sigma B_0^2}{\rho_f}v\right).\#(3)$$

$$u\frac{\partial T}{\partial r}+w\frac{\partial T}{\partial z}=\frac{\kappa}{(\rho c_p)_f}\frac{\partial^2 T}{\partial z^2}+\tau\left(\frac{D_T}{T_\infty}\left(\frac{\partial T}{\partial z}\right)^2+DB\ \frac{\partial T}{\partial z}\frac{\partial C}{\partial z}\right)+\frac{16\sigma_\star T_\infty^3}{3k_\star(\rho c_p)_f}\frac{\partial^2 T}{\partial z^2}+$$
$$\frac{\mu_f}{(\rho c_p)_f}\left(\left(\frac{\partial u}{\partial z}\right)^2+\left(\frac{\partial v}{\partial z}\right)^2\right)+\frac{Q_0}{(\rho c_p)_f}(T-T_\infty). \quad \#(4)$$

$$u\frac{\partial C}{\partial r}+w\frac{\partial C}{\partial z}=DB\ \frac{\partial^2 C}{\partial z^2}+\frac{DT}{T_\infty}\left(\frac{\partial^2 T}{\partial z^2}\right)-k_r(C-C_\infty)\left(\frac{T}{T_\infty}\right)^b\exp\left(-\frac{\mathrm{EA}}{\lambda\ T}\right).\#(5)$$

$$u\frac{\partial S}{\partial r}+w\frac{\partial S}{\partial z}+\frac{JHC}{C_f-C_\infty}\left[\frac{\partial}{\partial z}\left(S\frac{\partial C}{\partial z}\right)\right]=Ds\frac{\partial^2 S}{\partial z^2}.\#(6)$$

Where M_y and M_x are expressed as:

$$M_y = \left(u^2\frac{\partial^2 v}{\partial r^2} + 2uv\frac{1}{r}\frac{\partial u}{\partial r} - \frac{2u^2 v}{r^2} + 2uw\frac{\partial^2 v}{\partial r \partial z} - \frac{v^3}{r^2} + 2vw\frac{1}{r}\frac{\partial u}{\partial z} + \frac{v^2}{r}\frac{\partial v}{\partial r} + w^2\frac{\partial^2 v}{\partial z^2}\right) \quad \#(7)$$

$$M_x = \left(u^2\frac{\partial^2 u}{\partial r^2} - 2uv\frac{1}{r}\frac{\partial v}{\partial r} + \frac{uv^2}{r^2} + 2uw\frac{\partial^2 u}{\partial r \partial z} - 2vw\frac{1}{r}\frac{\partial v}{\partial z} + w^2\frac{\partial^2 u}{\partial z^2} + \frac{v^2}{r}\frac{\partial u}{\partial r}\right) \quad (8)$$

The relevant wall conditions for the controlling equations are:

$$\begin{cases} \mu_f\left(\dfrac{\partial u}{\partial z}\right) = \dfrac{\partial \sigma}{\partial T}\dfrac{\partial T}{\partial r} + \dfrac{\partial \sigma}{\partial C}\dfrac{\partial C}{\partial r} + \dfrac{\partial \sigma}{\partial S}\dfrac{\partial S}{\partial r}, & \\ v = ar, w = 0, -\kappa\dfrac{\partial T}{\partial z} = h_f(T_f - T), C = C_w, S = S_w, & \text{at } z = 0, \\ u \to 0, v \to 0, T \to T_\infty, C \to C_\infty, S \to S_\infty, & \text{as } z \to \infty. \end{cases} \quad \#(9)$$

Where

$$\sigma = \sigma_0 - \left(\frac{\partial \sigma}{\partial T}\right)_{T=T_\infty}[(T - T_\infty)] - \left(\frac{\partial \sigma}{\partial C}\right)_{C=C_\infty}[(C - C_\infty)] + \left(\frac{\partial \sigma}{\partial S}\right)_{S=S_\infty}[(S - S_\infty)] \quad (10)$$

The symbols featuring in equations (1-10) are defined in Table 1.

Table 1: Definition and symbols description

Letter	Definition	Letter	Definition
u, v, w	Velocity components	C	concentration
DB	Brownian motion coefficient	C_0	reference concentration
DT	thermophoresis factor	C_∞	upstream concentration
T	Temperature	$K^\star$	Permeability of porous medium
T_0	Reference temperature	S	density of motile microorganisms,
κ	thermal conductivity	S_0	Reference motile microorganisms,
τ	heat capacity ratio,	S_∞	motile microorganisms at ambient
ρ_f	fluid density	B_0	magnetic field strength
μ_f	dynamic viscosity	a	disk rotation rate
λ_1	fluid relaxation time	σ_0	electrical conductivity
c_p	specific heat capacity	ω	magnetic inclination angle
h_s	convective heat transfer	EA	activation energy coefficient
Q_0	Coefficient of heat source	kr	Chemical reaction rate
HC	Chemotaxis constant	DS	Diffusivity of microorganisms

Quantities of Similarity Transformation

Equation (11) consists of the variables employed to remodel equations (1-6) together with (9) into ordinary derivatives, and the dimensionless physical quantities emanated from the equations.

$$u = arf'(\eta), v = arg(\eta), \frac{w}{f(\eta)} = -2\sqrt{a\vartheta_f}\,,\ T_0 r^2\theta = T - T_\infty = \frac{T - T_\infty}{T_f - T_\infty},$$

$$C_0 r^2\phi = C - C_\infty \to \frac{C - C_\infty}{C_f - C_\infty}, S_0 r^2 h = S - S_\infty \to \frac{S - S_\infty}{S_f - S_\infty}, \frac{\eta}{z} = \left(\frac{a}{\vartheta_f}\right)^{0.5}$$

$$M_0 = \frac{H_t\, A}{\mu_f\, a\, r^2}\sqrt{\frac{\upsilon_f}{a}},\quad R_n = \frac{H_n\, B}{H_t\, A},\quad R_S = \frac{H_S\, C}{H_t\, A},\quad \alpha = \frac{h_s}{k_\infty}\sqrt{\frac{\vartheta_f}{a}},\quad \beta = a\,\lambda_1, L = \frac{\vartheta_f}{a\,K^*},$$

$$M = \frac{\sigma\, B_0^2}{\rho_f\, a},\quad Pr = \frac{(\mu c_p)_f}{k_\infty},\quad Nt = \frac{\tau\, D_T T_0 r^2}{T_\infty \upsilon_f}, Nb = \frac{\tau\, D_B C_0 r^2}{\vartheta_f}, Ec = \frac{a^2 r^2}{c_p T_0 r^2},$$

$$Nr = \frac{16\sigma_* T_\infty^3}{3k_* k_\infty},\quad \gamma = \frac{k_r}{a},\quad \in = \frac{EA}{\lambda\ T_\infty},\quad Lb = \frac{\upsilon_f}{D_m},$$

$$Pe = \frac{J\, W_c}{D_m},\quad q = \frac{S_\infty}{S_f - S_\infty},\quad Q = \frac{Q_0}{a\,(\rho c_p)_f},\quad Sc = \frac{\vartheta_f}{D_B}.$$

$$\#(11)$$

By incorporating (11), the controlling equations become ordinary derivatives as follows:

$$f''' - 4\beta(f^2 f''' - ff'f'' - fgg') - (f'^2 - 2ff'' - g^2) - (Lf' + Mf') = 0, \#(12)$$

$$g'' - 4\beta(f^2 g'' - ff'g' - ff''g) - 2(f'g - fg') - (Lg + Mg) = 0, \#(13)$$

$$[1 + Nr]\theta'' - 2Pr(f'\theta - f\theta') + Pr(Nt\theta'^2 + Nb\theta'\phi') + PrQ\theta + PrEc(f''^2 + g'^2) = 0, \#(14)$$

$$\phi'' - 2Sc(f'\phi - f\phi') + \frac{Nt}{Nb}\theta'' - Sc\gamma \ (1+\theta)^{b}\exp\left(\frac{-\epsilon}{1+\theta}\right)\phi = 0. \#(15)$$

$$h'' - 2Lb(f'h - 2fh') - Pe[h'\phi' + \phi''(h+q)] = 0. \#(16)$$

Subject to:

$$\left\{\begin{array}{l} f''(0) + 2M_0(1 + R_n + R_s), g(0) - 1 = 0, f(0) = 0, \\ \theta'(0) + \alpha(1 - \theta(0)) = 0, h(0) - 1 = 0, \phi(0) - 1 = 0, \\ f'(\eta) \to 0, g(\eta) \to 0, \theta(\eta) \to 0, \phi(\eta) \to 0, h(\eta) \to 0, \quad \text{as } \eta \to \infty. \end{array}\right. \#(17)$$

The parameters emanated from the dimensionless equations (12-17) are recorded in Table 2.

Table 2: parameters description

Parameter	Definition	Parameter	Definition
M	Magnetic field	Nb	Brownian motion
M_0	Thermal Marangoni number	Rd	Radiation
L	Porosity factor	Sc	Schmidt number
R_n	Solutal Marangoni number	Ec	Eckert number
R_s	Motile Marangoni number	Pr	Prandtl number
α	Biot number	$\in$	Activation energy
Nt	Thermophoresis	Pe	Peclet number
Q	Heat generation	Lb	Bioconvective Lewis number
γ	Chemical reaction	β	Deborah number

Furthermore, the physical quantities for engineering applications are defined as the skin friction coefficient (C_{fr}), Nusselt number (Nu_r),and Sherwood number (Sh_r). These are sequentially stated in equation (19) as:

$$\left.\begin{array}{l} C_{fr} = \frac{(\tau_{zr}^2 + \tau_{z\varphi}^2)^{1/2}}{\rho_f(\zeta r)^2}, \quad Nu_r = \frac{r\, q_w}{k_\infty(T_f - T_\infty)}, \quad Sh_r = \frac{r\, j_w}{D_B(N_f - N_\infty)}, \end{array}\right\} \quad (19)$$

with

$$\left.\begin{array}{l} \tau_w = \mu_f\left[\left(\frac{\partial u}{\partial z}\right)^2 + \left(\frac{\partial v}{\partial z}\right)^2\right]^{\frac{1}{2}}, \quad q_w = -\left[k(T) + \frac{16\sigma_* T_\infty^3}{3k_*}\right]\left(\frac{\partial T}{\partial z}\right)_{z=0}, \\ j_w = -D_B\left(\frac{\partial N}{\partial z}\right)_{z=0}, \quad j_s = -D_S\left(\frac{\partial S}{\partial z}\right)_{z=0}, \end{array}\right\} \quad (20)$$

The non-dimensional forms of (17) are:

$$\left.\begin{array}{l} C_{fr}Re_r^{\frac{1}{2}} = 2[f''(0) + g'(0)], \\ Nu_r Re_r^{-\frac{1}{2}} = -(1 + Rd)\ )\ \theta'(0), \\ Sh_r Re_r^{-\frac{1}{2}} = -\phi'(0). \end{array}\right\} \quad (21)$$

where $Re_r = a\, r^2/\upsilon_f$ is the local Reynolds number

Solution Methodology and Validation of Results

Equations (12-17) represent high nonlinear stiff equations with no feasible closed form solution. Thus, the required solution to the set of these equations is sought numerically via shooting method together with Runge-Kutta Felhberg integration techniques. The mathematical formulation consisting of equations (12)–(16) and the associated boundary conditions in (17) describes a nonlinear problem whose conditions are specified at two separate boundaries (as the boundary conditions for the nonlinear system are defined at two separate points $\eta = 0$ and $\eta \to \infty$). For numerical treatment, the formulation is first converted into an equivalent initial value problem, after which the shooting approach is employed to compute the solutionwith the RKF45 integration method, The first order ODEs will be formed by converting the higher order ODEs to first order ODEs and done by transforming the following variables into first order ODEs.

$$y_1 = f, \quad y_2 = f', y_3 = f'', y_4 = g, \quad y_5 = g',$$
$$y_6 = \theta, \quad y_7 = \theta', \quad y_8 = \phi, \quad y_9 = \phi',$$
$$y_{10} = h, \quad y_{11} = h'$$

With these substitutions, the resulting equations are reduced to a system of eleven coupled first-order differential equations, which are appropriate for numerical computation. Next, the boundary conditions applied at η = 0 are directly applied. However, some of the initial conditions such as $f''(0), g'(0), \theta'(0), \phi'(0)$, and $h'(0)$ are unknown in advance. These unknowns are treated as shooting parameters, and appropriate initial guesses are assigned to them.Then, the Initial Value Problem can be integrated from $\eta = 0$ to η_∞, which is large enough to be a good approximation for the boundary at infinity. The integration is performed with the Runge-Kutta-Fehlberg (RKF45) method using the symbolic algebra Maple software. An adaptive step-size control that combines both fourth and fifth order R-K formulas provides a stable and accurate solution to the IVP with a minimum amount of truncation error.

The computed values of the dependent variables at η∞ are compared with the specified boundary conditions at the far field $: f'(\eta) \to 0, g(\eta) \to 0, \theta(\eta) \to 0, \phi(\eta) \to 0, h(\eta) \to 0 \; as \; \eta \to \infty$. If the above-specified boundary conditions are not satisfied, the shooting parameters are updated, and the integration is repeated with new guesses for the parameters using a secant method or Newton-Raphson method. After achieving the convergence criteria, the numerical solutions for the velocity components, temperature distribution, nanoparticle concentration, and density of the motile microorganisms are obtained, and the results are used to study the influence of the involved parameters and to obtain the graphical and tabular results as presented in this paper. Under some limiting scenarios, the results obtained for variation of the magnetic field term are in proper agreement with existing related data in the literature as shown in Table 3.

Table 3: Computed values of the skin friction factor for variation in M when $\beta = 0.01, \omega = \pi/3$

M	Devi & Mabood (2020)	Current study
0	1.385853	1.385863
0.4	1.445328	1.445368
0.8	1.51867	1.518871

Analysis of Results and Discussion

Under this section, some graphs are sketched to showcase the impacts of selected key parameters on the flow field.

Figures 2 and 3 represent the behaviour of the velocity fields as M magnifies in strength.The profiles exhibit a downward trend in both directions (radial and tangential) as M rises. A rise M causes a drag in the floe field due to the action of the Lorentz force, which opposes the electrically conducting fluid motion. The attenuation is more significant in the radial direction than in the tangential direction as depicted in these figures. Radial motion, being primarily induced by centrifugal forces, is more susceptible to magnetic braking; resulting in widely separated radial velocity profiles.

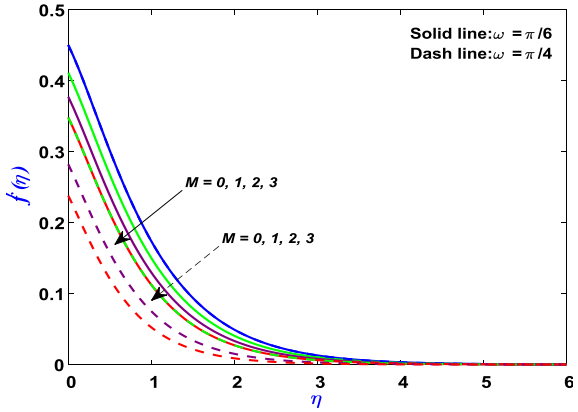

Figure 2: Radial velocity for variation of M

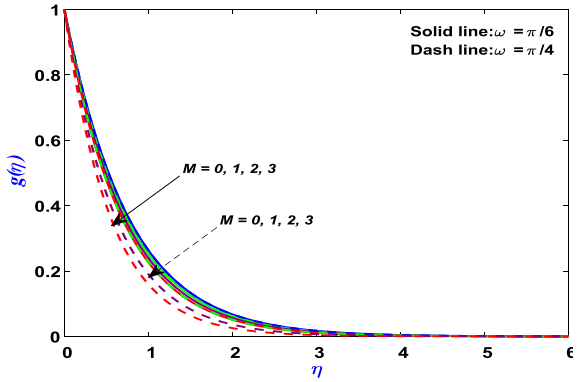

Figure 3: Tangential velocity for variation of M

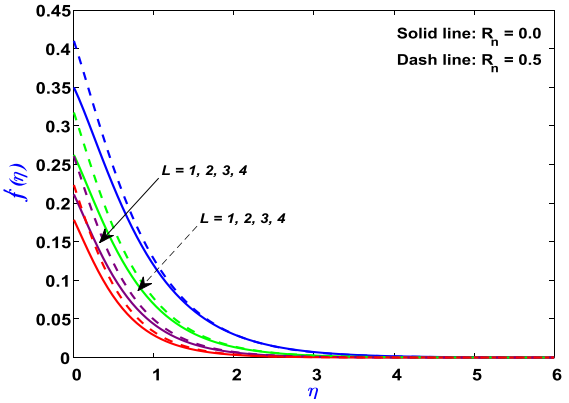

Figure 4: Radial velocity for porosity term L

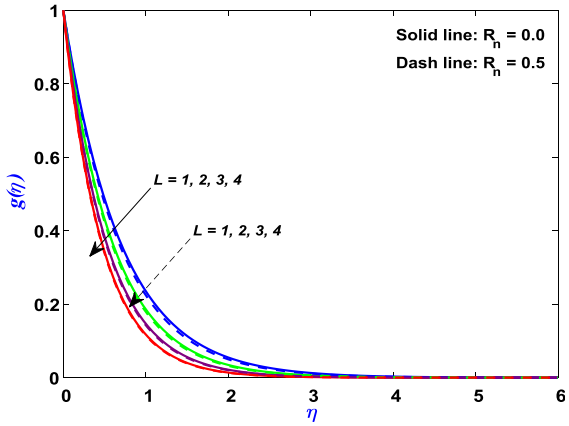

Figure 5: Tangential velocity for porosity term L

Furthermore, a rise in the inclination angle enhances the effective magnetic field strength interacting with the flow, intensifying magnetic damping and further suppressing both radial and tangential velocities. A decline occurs in the velocity profiles in both directions as L rises (Figs 4 and 5). The occurrence of this trend is due to the additional resistance introduced by the porous medium, which opposes momentum transfer and restricts the free flow of the Maxwell nanofluid. The sensitivity of the radial velocity is due to the fact that it is controlled mainly by the centrifugal effects, whereas the tangential velocity is maintained partially by the disk rotation. Such results are important for various branches of engineering, such as solar collectors with porous absorbers, filtration devices, and the intensification of cooling processes for rotating machines.

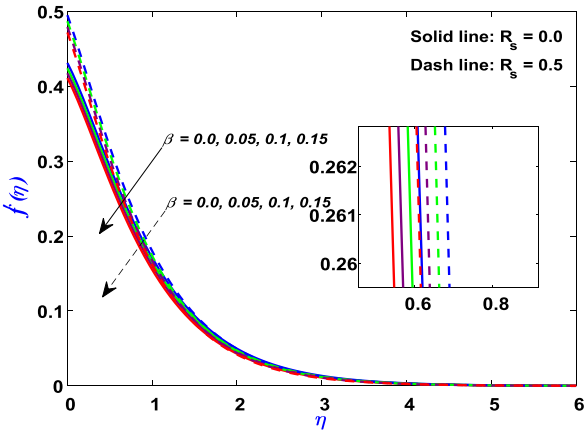

Figure 6: Flow pattern for Deborah number

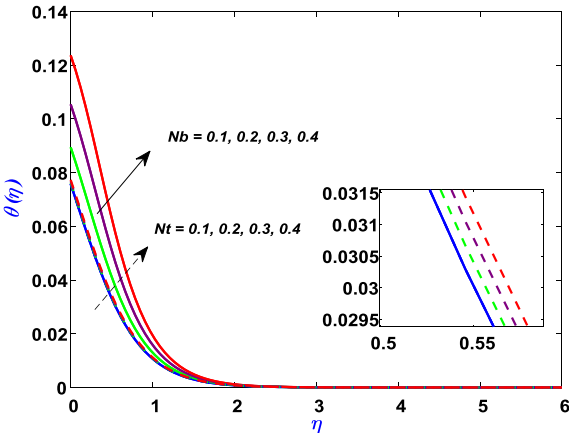

Figure 7: Heat trend for changes in Nb & Nt

The picture in Figs 6 and 7 reveal the declining nature of the velocity field due to the amplifying values of the Deborah number β. The decreasing effect exhibited in this Figure is due to the fact rising pattern of βimplies higher elasticity of the Maxwell fluid material, which resists deformation and slows momentum transfer.

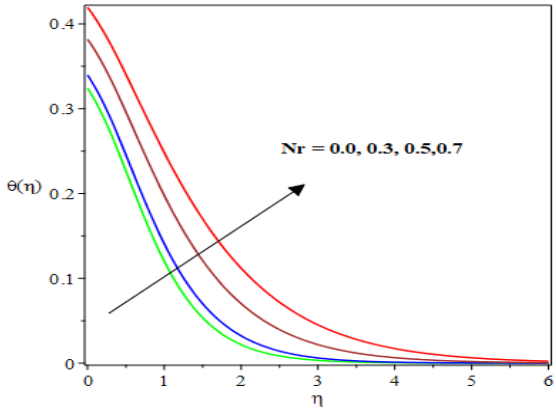

Figure 8: Heat profile for radiation $term$ (Nr)

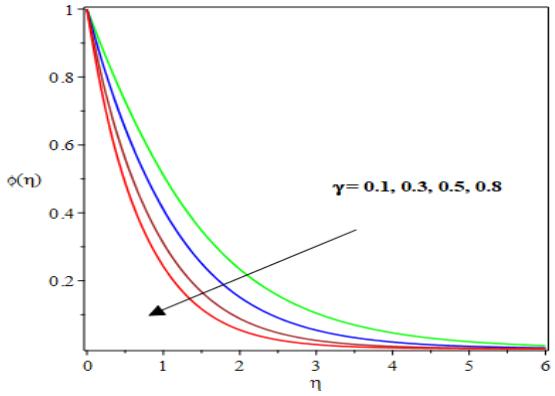

Figure 9: Concentration profile for variation inγ

These findings are important for regulating the elastic behaviour of the fluid, which assists in achieving better flow distribution, improving heat transfer performance, and minimizing excessive shear stress within the system. Such control is particularly relevant in practical applications including rotating disk heat exchangers, polymer manufacturing processes, thin-film coating technologies, and the thermal management of rotating mechanical components. Fig. 7 exhibit the impact of Nb and Nt on the temperature distribution. An increase in both parameters leads to a thicker thermal wall which also enables an elevation in the temperature of the Maxwell nanofluid. The random movement of nanoparticles caused by Brownian motion enhances the transport of thermal energy, whereas thermophoretic forces drive particles from high-temperature regions toward cooler zones, thereby strengthening thermal diffusion. These mechanisms play a significant role in systems such as solar energy collectors, electronic cooling devices, and heat exchangers, where improved nanoparticle heat transport can enhance overall thermal efficiency. Fig. 8 presents the variation in temperature distribution with respect to the radiation parameter Nr. Increasing Nr intensifies the radiative heat transfer, which enlarges the thermal boundary layer and raises the temperature within the fluid region. Conversely, higher values of the chemical reaction parameter γ reduce the thickness of the concentration (solutal) boundary layer.

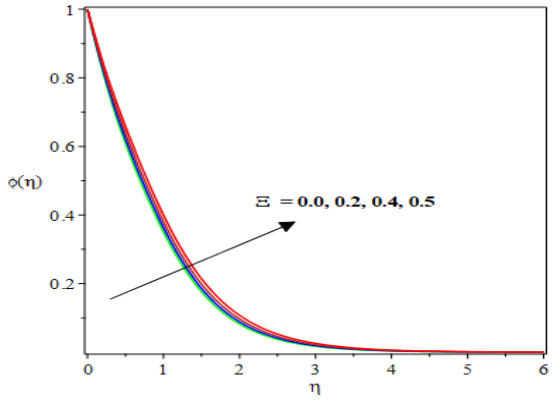

Figure 10: Concentration profile for variation∈

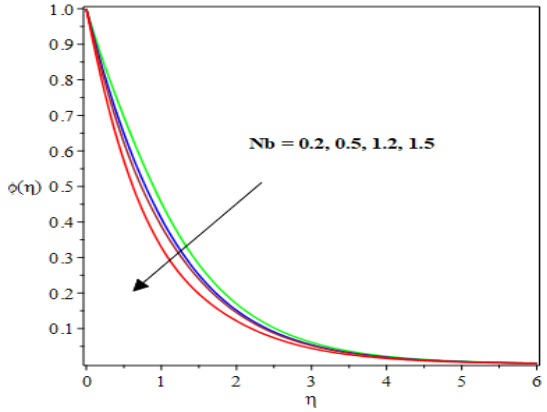

Figure 11: Concentration profile for *Nb*

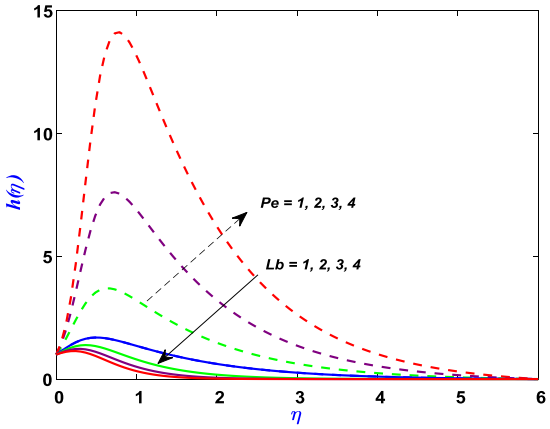

Figure 12: Microorganism profiles for *Pe* & *Lb*

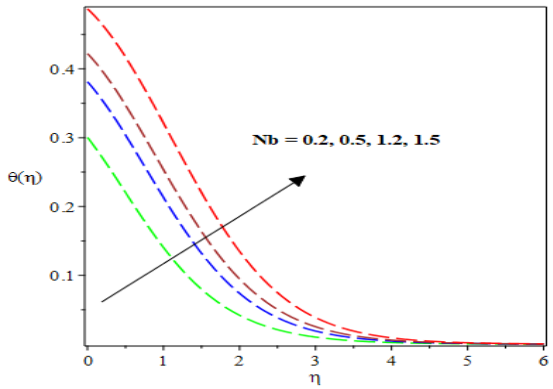

Figure 13: Concentration profiles for *Nb*

A rise in activation energy term ϵ promotes a rise in the concentration field as described pictorially in Fig. 10. This resulted from the fact that an increase with an increase in ϵ, the nanoparticle concentration profile suppresses the chemical reaction rate, and as such, the species consumption rate is reduced.

The impact of both the Peclet and bioconvection Lewis numbers on the microorganism profiles are illustrated in Fig. 12. It is revealed that a rise in Pe boosts the speed of the microorganisms, whereas the opposite trend is exhibited by Lb. Physically, with a rise in Pe, the advective transport of motile microorganisms is strengthened relative to diffusion, thus, more microorganisms migrate along the flow and accumulate in the boundary layer. With arise $in\ Lb$, there is an increase in the microorganism diffusivity relative to the fluid viscosity, as this happens, the microorganisms are dispersed more rapidly and reduces the bioconvective accumulation, resulting in lower concentration profiles.

CONCLUSION

In the present investigation, the dynamics of hydromagnetic Maxwell nanofluid flow over a spinning disk with Marangoni convection are examined. The model also incorporates the effects of medium porosity, thermal radiation, chemical reaction, and bioconvection. The governing model equations are solved numerically using the shooting technique in conjunction with the Runge–Kutta–Fehlberg scheme. The results reveal the influence of key physical parameters on the velocity, temperature, and concentration profiles. The outcomes of this study are useful for optimizing flow control, heat and mass transport, and the overall thermal efficiency of the system. Such improvements are important for various practical and technological applications, including solar energy systems, heat exchangers, and rotating mechanical devices. From the current investigation, it is found that increasing the Maxwell fluid material parameter (β) leads to a reduction in the velocity field because it suppresses elastic deformation effects, thereby influencing shear stress distribution and aiding in momentum control within the flow system. Similarly, an increase in the porosity parameter (L) results in a decrease in both radial and tangential velocity profiles due to enhanced resistive forces associated with the porous medium, with the effect being more pronounced in the radial direction as a result of centrifugal influences. In terms of thermal characteristics, both thermophoresis and Brownian motion parameters contribute to an increase in the thermal boundary layer thickness and fluid temperature, as particle random motion and temperature-gradient-driven migration intensify energy transport within the system. In addition, higher thermal radiation (Nr) enhances the temperature profile by increasing radiative heat transfer, which in turn strengthens both conductive and convective heat transfer processes at the surface. For mass transfer behaviour, an increase in the chemical reaction parameter (γ) leads to a reduction in

the solutal boundary layer thickness due to enhanced species consumption, whereas an increase in activation energy (ϵ) enhances nanoparticle concentration by inhibiting the rate of chemical reaction and reducing depletion effects.

Finally, an increase in the Peclet number (Pe) enhances microorganism advection, leading to greater accumulation of motile microorganisms within the fluid, while an increase in the bioconvection Lewis number (Lb) strengthens diffusion effects, promoting greater dispersal of microorganisms and reducing localized concentration build-up. The results derived from this study have wide-ranging applications in various fields, including: Optimization of solar energy collectors with porous absorbers for better heat transfer. Improvement of heat exchanger cooling systems, as well as the cooling systems of rotating machinery, through flow control. Bioconvective flow control in bio-nano fluid systems for better flow mixing. In summary, the results of this study show that the optimization of porosity, fluid elasticity, nanoparticle behaviour, thermal radiation, chemical reaction, and bioconvection can significantly optimize the flow, resulting in better heat and mass transfer.

Conflict of interest: The authors declare no conflicts of interest.

REFERENCES

Abdelsalam, S. I., Abbas, W., Megahed, A. M. and Said, A. A. (2023). A comparative study on the rheological properties of upper convected Maxwell fluid along a permeable stretched sheet. Heliyon, 9(12), e22740. https://doi.org/10.1016/j.heliyon.2023.e22740

Acharya, N., Mabood, F., Shahzad, S. A. and Badruddin, I. A. (2022). Hydrothermal variations of radiative nanofluid flow by the influence of nanoparticles diameter and nanolayer. International Communications in Heat and Mass Transfer, 130, 105781. https://doi.org/10.1016/j.icheatmasstransfer.2021.105781

Alrihieli, H., Aldhabani, M. S., Alshaban, E. and Alatawi, A. (2025). Thermal-hydrodynamic analysis of a Maxwell fluid with controlled heat/mass transfer over a Riga plate: A numerical study with engineering applications. *Results in Engineering*, 26, 104801. https://doi.org/10.1016/j.rineng.2025.104801

Alsallami, H., Alghamdi, M. and Khan, M. (2020). Marangoni convection in nanofluid flow over stretching surfaces with thermal radiation effects. *Applied Mathematics and Mechanics*, 41(8), 1153–1166. https://doi.org/10.1007/s10483-020-2634-7

Buongiorno, J. (2006). Convective transport in nanofluids. *Journal of Heat Transfer*, 128(3), 240–250. https://doi.org/10.1115/1.2150834

Chebaane, S., Fatunmbi, E. O., Obalalu, A. M., Al Qawasmeh, A., Manai, L. and Azhary, A. (2025). Influence of gyrotactic microorganisms and thermophoretic effects on two-phase nanofluid transport over wedge surfaces in Carreau and Casson liquids. *Journal of Thermal Analysis and Calorimetry*, 150(20), 16271-16286. https://doi.org/10.1007/s10973-025-14669-9

Choi, S. U. S. and Eastman, J. A. (1995). Enhancing thermal conductivity of fluids with nanoparticles. *ASME Int. Mechanical Engineering Congress & Exposition, San Francisco*, 22, 12–17.

Devi, S. S. U. and Mabood, F. (2020). Entropy anatomization on Marangoni Maxwell fluid with nonlinear radiation and activation energy. *Int. Communic. in Heat and Mass Tran*, 118, 104857. https://doi.org/10.1016/j.icheatmasstransfer.2020.104857

Fatunmbi, E. O. and Adeniyan, A. (2018). MHD stagnation point-flow of micropolar fluids past a permeable stretching plate in porous media with thermal radiation, chemical reaction and viscous dissipation. *Journal of Advanced Mathematics and Computational Science*, 26(1), 1–19.

Fatunmbi, E. O. and Adeniyan, A. (2020). Nonlinear thermal radiation and entropy generation on steady flow of magneto-micropolar fluid passing a stretchable sheet with variable properties. *Results in Engineering*, 6, 100142. https://doi.org/10.1016/j.rineng.2020.100142

Fatunmbi, E. O. and Agbolade, O. A. (2023). Quadratic thermal convection in Magneto-Casson fluid flow induced by stretchy material with tiny particles and viscous dissipation effects. *Physical Science International Journal*, 27(4) 1-11. https://doi.org/10.9734/psij/2023/v27i4795

Fatunmbi, E. O. and Salawu, S. O. (2022). Analysis of hydromagnetic micropolar nanofluid flow past a nonlinear stretchable sheet and entropy generation with Navier slips. *Int. J. of Modelling and Simulation*, 42(3), 359-369. https://doi.org/10.1080/02286203.2021.1905490

Fatunmbi, E. O., Oke, A. S. and Salawu, S. O. (2023). Magnetohydrodynamic micropolar nanofluid flow over a vertically elongating sheet containing gyrotactic microorganisms with temperature-dependent viscosity. *Results in Materials*, 19, 100453. https://doi.org/10.1016/j.rinma.2023.100453

Fatunmbi, E. O., Ramonu, O. J. and Salawu, S. O. (2023). Analysis of heat transfer phenomenon in hydromagnetic micropolar nanoliquid over a vertical stretching material featuring convective and isothermal heating conditions. Waves in Random and Complex Media, 1-20. https://doi.org/10.1080/17455030.2023.2245678

Gul, T., Ahmed, Z., Jawad, M., Saeed, A. and Alghamdi, W. (2021). Bio-convectional nanofluid flow due to the thermophoresis and gyrotactic microorganism between the gap of a disk and cone. *Brazilian Journal of Physics*, 51(3), 687-697. https://doi.org/10.1007/s13538-021-00897-5

Guo, N., Yu, L., Shi, C., Yan, H. and Chen, M. (2024). A facile and effective design for dynamic thermal management based on synchronous solar and thermal radiation regulation. *Nano Letters*, 24(4), 1447-1453. https://doi.org/10.1021/acs.nanolett.3c04521

Hayat, T., Waqas, M., Shehzad, S. A. and Alsaedi, A. (2015). Effects of thermal radiation on magnetohydrodynamic flow of Maxwell nanofluid. *Journal of Molecular Liquids*, 204, 47–52. https://doi.org/10.1016/j.molliq.2015.01.002

Huminic, G. and Huminic, A. (2020). Entropy generation of nanofluid and hybrid nanofluid flow in thermal systems: a review. *Journal of Molecular Liquids*, 302, 112533. https://doi.org/10.1016/j.molliq.2020.112533

Lin, L., Liu, Y. and Zhang, X. (2019). Thermocapillary flow induced by Marangoni effects in rotating disk systems. *International Journal of Heat and Mass Transfer*, 132, 850–858. https://doi.org/10.1016/j.ijheatmasstransfer.2018.12.040

Mahian, O., Kolsi, L., Amani, M., Estellé, P., Ahmadi, G., Kleinstreuer, C., ... and Pop, I. (2019). Recent advances in modeling and simulation of nanofluid flows-Part I: Fundamentals and theory. *Physics Reports*, 790, 1-48. https://doi.org/10.1016/j.physrep.2018.11.004

Megahed, A. M. (2021). Improvement of heat transfer mechanism through a Maxwell fluid flow over a stretching sheet embedded in a porous medium and convectively heated. *Math & Computers in Simulation*, 187, 97–109. https://doi.org/10.1016/j.matcom.2021.02.018

Menni, Y., Chamkha, A. J. and Azzi, A. (2019). Nanofluid flow in complex geometries—a review. *Journal of Nanofluids*, 8(5), 893-916. https://doi.org/10.1166/jon.2019.1645

Mustafa, M., Hayat, T. and Alsaedi, A. (2017). Rotating flow of Maxwell fluid with variable thermal conductivity: an application to non-Fourier heat flux theory. *International Journal of Heat and Mass Transfer*, 106, 142-148. https://doi.org/10.1016/j.ijheatmasstransfer.2016.10.032

Nadeem, S., Ahmad, S., Muhammad, N. and Mustafa, M. T. (2017). Chemically reactive species in the flow of a Maxwell fluid. *Results in Physics*, 7, 2607-2613. https://doi.org/10.1016/j.rinp.2017.07.015

Nasir, S., Berrouk, A. and Khan, Z. (2024). Efficiency assessment of thermal radiation utilizing flow of advanced nanocomposites on Riga plate. *Applied Thermal Engineering*, 242, 122531. https://doi.org/10.1016/j.applthermaleng.2024.122531

Tiwari, R. K. and Das, M. K. (2007). Heat transfer augmentation in a two-sided lid-driven differentially heated square cavity utilizing nanofluids. *International Journal of Heat and Mass Transfer*, 50(9-10), 2002-2018. https://doi.org/10.1016/j.ijheatmasstransfer.2006.09.034

Wang, W., Xu, H. and Pop, I. (2016). Bioconvection of nanofluids containing gyrotactic microorganisms: A review. *Applied Mathematics and Mechanics*, 37(6), 687–706. https://doi.org/10.1007/s10483-016-2086-6

Yahaya, R. I., Mustafa, M. S., Arifin, N. M., Pop, I., Wahid, N. S., Ali, F. M. and Mohamed Isa, S. S. P. (2024). Mixed convection hybrid nanofluid flow over a stationary permeable vertical cone with thermal radiation and convective boundary condition. *ZAMM-Journal of Applied Mathematics and Mechanics*, 104(4), e202300428. https://doi.org/10.1002/zamm.202300428